

A P_1 CONFORMING DSA SCHEME FOR DGFEM S_N TRANSPORT

Yaqi Wang, Jean C. Ragusa
Department of Nuclear Engineering
Texas A&M University
College Station, TX, 77843-3133
yaqiwang@tamu.edu; ragusa@ne.tamu.edu

ABSTRACT

The consistency of the lower-order diffusion equations in Diffusion Synthetic Acceleration (DSA) is a crucial element for the stability and effectiveness of any DSA methods. A P_1 conforming DSA scheme is proposed for the S_N transport equations discretized in space using a Discontinuous Galerkin Finite Element Methods (DGFEM). The DSA scheme is obtained employing a variational argument. Comparisons of this conforming scheme with the mixed DGFEM form derived by Warsa, Wareing and Morel for the continuous P_1 equation are presented. Some preliminary results with a simple 2-cell problem suggest that this new form is stable and can also be applied to problems with highly anisotropic scattering.

Key Words: Diffusion Synthetic Acceleration, DSA, S_N transport, Discontinuous Galerkin Finite Element Method, DGFEM.

1. INTRODUCTION

The consistency of the lower-order diffusion equations in DSA (Diffusion Synthetic Acceleration) is a crucial element for the stability and effectiveness of any DSA methods [1]. A general requirement for consistency is that the DSA equations are derived from the discretized transport equation. In this work, we consider spatial discretization techniques based on Discontinuous Galerkin Finite Element Methods (DGFEM) and we propose to analyze DSA schemes that employ DGFEM discretization. In order to proceed, we first cast the S_N transport equation, spatially discretized with DGFEM and a standard upwinding procedure [3][4], into a variational form. We then reduce this variational form into a diffusion form by restricting the angular flux and basis test functions to be linear in angle. The resulting DSA form (which we denoted by DSA-P1C) form is slightly *different* from the mixed DGFEM form (DSA-P1M) obtained by Warsa and Morel [2] for the continuous P_1 equation. In DSA-P1M, the numerical scalar flux on any interface is defined as two times the summation of the two outgoing partial currents with respect to the two neighboring elements and the numerical net current crossing the interface is the difference between the two partial currents. Readers are referred to Ref. [2] for more implementation details. We observed some differences between the DSA-P1C and DSA-P1M forms that could have significant impact in highly anisotropic scattering cases.

In this paper, we first conduct the variational derivation to obtain the DSA-P1C from the DGFEM S_N

transport. Then, we point out the differences between the DSA-P1C and the DSA-P1M. We present some preliminary results with a simple 2-cell problem in the Results section. Finally, we propose some concluding remarks and highlight additional work and results to be included in the final paper.

2. THE P_1 FORMS

We first briefly present the variational form for the S_N transport. Then, a P_1 approximation is employed to arrive at the so-called DSA-P1C equations (the C stands for conforming).

2.1. Variational form for S_N transport with DGFEM

For simplicity, our presentation is carried out for the one-group S_N transport equation with only vacuum and reflecting boundaries. Given an angular quadrature set $\{\vec{\Omega}_m, w_m\}_{1 \leq m \leq M}$, the one-speed steady state S_N neutron transport equation in one direction m with anisotropic source and scattering, in a domain D with boundary $\partial D = \partial D^v \cup \partial D^r$ (vacuum and reflecting), is:

$$\begin{aligned} \vec{\Omega}_m \cdot \vec{\nabla} \Psi_m(\vec{r}) + \sigma_t(\vec{r}) \Psi_m(\vec{r}) &= \sum_{\ell, n} \frac{2\ell + 1}{4\pi} Y_{\ell, n}(\vec{\Omega}_m) [\sigma_{s, \ell}(\vec{r}) \Phi_{\ell, n}(\vec{r}) + Q_{\ell, n}(\vec{r})] \\ &\equiv q_m(\vec{r}) \text{ on } \mathcal{D} \end{aligned} \quad (1)$$

We used the notation $\Psi_m(\vec{r}) = \Psi(\vec{r}, \vec{\Omega}_m)$ and denoted the spherical harmonics by $Y_{\ell, n}$. The boundary conditions are:

$$\Psi_m(\vec{r}_b) = 0 \quad \text{on } \partial \mathcal{D}_m^{v-} = \left\{ \vec{r}_b \in \partial \mathcal{D}^v, \vec{\Omega}_m \cdot \vec{n}(\vec{r}_b) < 0 \right\} \quad (2)$$

$$\Psi_m(\vec{r}_b) = \Psi_{m'}(\vec{r}_b) \quad \text{on } \partial \mathcal{D}_m^{r-} = \left\{ \vec{r}_b \in \partial \mathcal{D}^r, \vec{\Omega}_m \cdot \vec{n}(\vec{r}_b) < 0 \right\} \quad (3)$$

where the reflected direction is given by:

$$\vec{\Omega}_{m'} = \vec{\Omega}_m - 2(\vec{\Omega}_m \cdot \vec{n}(\vec{r}_b))\vec{n}(\vec{r}_b) \quad (4)$$

A mesh \mathbb{T}_h is used to discretize the domain \mathcal{D} into linear elements K (specifically triangles in our applications), such that the union of all elements fully covers \mathcal{D} , i.e., $\bigcup_{K \in \mathbb{T}_h} K = \mathcal{D}$. Letting E_h^i be the set of all interior faces (edges in 2-D), we write down the variational form of DGFEM for Eq. (1) for all directions and linearly combine (add) them using $4\pi w_m$ as weights:

$$\begin{aligned}
 b(\Psi, \Psi^*) &= \sum_{K \in \mathbb{T}_h} \sum_{m=1}^M 4\pi w_m ((\vec{\Omega}_m \cdot \vec{\nabla} + \sigma_t) \Psi_m, \Psi_m^*)_K \\
 &+ \sum_{e \in E_h^i} \sum_{m=1}^M 4\pi w_m ([\Psi_m], \Psi_m^{*+})_e + \sum_{e \in \partial \mathcal{D}} \sum_{\vec{\Omega}_m \cdot \vec{n}_e < 0} 4\pi w_m (\Psi_m, \Psi_m^*)_e \\
 &- \sum_{\ell, n} \sum_{K \in \mathbb{T}_h} (\sigma_{s, \ell} \Phi_{\ell, n}, \Phi_{\ell, n}^*)_K - \sum_{e \in \partial \mathcal{D}^r} \sum_{\vec{\Omega}_m \cdot \vec{n}_e < 0} 4\pi w_m (\Psi_{m'}, \Psi_m^*)_e
 \end{aligned} \tag{5}$$

$$l(\Psi^*) = \sum_{\ell, n} \sum_{K \in \mathbb{T}_h} (Q_{\ell, n}, \Phi_{\ell, n}^*)_K \tag{6}$$

Both the primal and adjoint functional spaces are identical and consist of piece-wise discontinuous polynomials.

We used the following definitions for the interior interface terms:

$$\Psi_m^+ = \lim_{s \rightarrow 0^+} \Psi(\vec{r} + s\vec{\Omega}_m) \tag{7}$$

$$\Psi_m^- = \lim_{s \rightarrow 0^-} \Psi(\vec{r} + s\vec{\Omega}_m) \tag{8}$$

$$[[\Psi_m]] = \Psi_m^+ - \Psi_m^- \tag{9}$$

On the boundary faces (edges), both the solution and test function are obtained from within the computational domain.

The element and face (edge) inner products are defined by:

$$(f, g)_K \equiv \int_K f g d^3 r \tag{10}$$

$$(f_m, g_m)_e \equiv \int_e |\vec{\Omega}_m \cdot \vec{n}_e| f_m g_m d^2 r \tag{11}$$

2.2. The P1C Form (DSA-P1C)

If we substitute in Eq. (6) the standard P_1 approximation

$$\Psi_m = \frac{1}{4\pi} (\Phi + 3\vec{J} \cdot \vec{\Omega}_m) \tag{12}$$

$$\Psi_m^* = \frac{1}{4\pi} (\Phi^* + 3\vec{J}^* \cdot \vec{\Omega}_m), \tag{13}$$

we obtain, after some lengthy algebra,

$$\begin{aligned}
b_{DSA-P1C}(\Phi, \vec{J}, \Phi^*, \vec{J}^*) &= (\sigma_a \Phi, \Phi^*)_{\mathcal{D}} + (3\sigma_{tr} \vec{J}, \vec{J}^*)_{\mathcal{D}} + (\vec{\nabla} \Phi, \vec{J}^*)_{\mathcal{D}} - (\vec{J}, \vec{\nabla} \Phi^*)_{\mathcal{D}} \\
&+ \frac{1}{4}([\Phi], [\Phi^*])_{E_h^i} + ([\Phi], \{\{\vec{J}^* \cdot \vec{n}\}\})_{E_h^i} - (\{\{\vec{J} \cdot \vec{n}\}\}, [\Phi^*])_{E_h^i} \\
&+ \frac{9}{16}([\vec{J} \cdot \vec{n}], [\vec{J}^* \cdot \vec{n}])_{E_h^i} + \frac{9}{16}([\vec{J}], [\vec{J}^*])_{E_h^i} \\
&+ \frac{1}{4}(\Phi, \Phi^*)_{\partial \mathcal{D}^v} + \frac{1}{2}(\vec{J} \cdot \vec{n}, \Phi^*)_{\partial \mathcal{D}^v} - \frac{1}{2}(\Phi, \vec{J}^* \cdot \vec{n})_{\partial \mathcal{D}^v} \\
&+ \frac{9}{16}(\vec{J}, \vec{J}^*)_{\partial \mathcal{D}^v} + \frac{9}{16}(\vec{J} \cdot \vec{n}, \vec{J}^* \cdot \vec{n})_{\partial \mathcal{D}^v} \\
&+ \frac{9}{4}(\vec{J} \cdot \vec{n}, \vec{J}^* \cdot \vec{n})_{\partial \mathcal{D}^r}
\end{aligned} \tag{14}$$

$$l(\Phi^*, \vec{J}^*) = (Q_0, \Phi^*)_{\mathcal{D}} + (3\vec{Q}_1, \vec{J}^*)_{\mathcal{D}} \tag{15}$$

where we have made some standard assumptions related to the angular quadrature:

$$\sum_{m=1}^M w_m = 4\pi \tag{16}$$

$$\sum_{m=1}^M w_m \vec{\Omega}_m = 0 \tag{17}$$

$$\sum_{m=1}^M w_m \vec{\Omega}_m \vec{\Omega}_m = \frac{4\pi}{3} I \tag{18}$$

$$\sum_{m=1}^M w_m \vec{\Omega}_m \vec{\Omega}_m \vec{\Omega}_m = 0 \tag{19}$$

$$\sum_{\vec{\Omega}_m \cdot \vec{n} > 0} w_m |\vec{\Omega}_m \cdot \vec{n}| = \pi \tag{20}$$

$$\sum_{\vec{\Omega}_m \cdot \vec{n} > 0} w_m |\vec{\Omega}_m \cdot \vec{n}| \vec{\Omega}_m = \frac{2\pi}{3} \vec{n} \tag{21}$$

$$\sum_{\vec{\Omega}_m \cdot \vec{n} > 0} w_m |\vec{\Omega}_m \cdot \vec{n}| \vec{\Omega}_m \vec{\Omega}_m = \frac{\pi}{4} (I + \vec{n} \vec{n}) \tag{22}$$

The \vec{Q}_1 term represents the first angular moments for the external source. We used the following definitions for the interface scalar flux (and similar equations for the current terms),

$$\Phi^+ = \lim_{s \rightarrow 0^+} \Phi(\vec{r} + s\vec{n}) \quad (23)$$

$$\Phi^- = \lim_{s \rightarrow 0^-} \Phi(\vec{r} + s\vec{n}) \quad (24)$$

$$[[\Phi]] = \Phi^+ - \Phi^- \quad (25)$$

$$\{\{\Phi\}\} = (\Phi^+ + \Phi^-)/2 \quad (26)$$

On the boundaries, there is no ambiguity for \vec{n} , which always points outwards. The orientation \vec{n} for an interior face (edge in 2D) is arbitrary since it does not change the result in the above formula. This form is denoted as P1C (P_1 Conforming Form).

2.3. Mixed DGFEM Form, DSA-P1M

For comparison purposes, we also provide the mixed DGFEM form (P1M), as presented in Ref. [2]:

$$\begin{aligned} b_{DSA-P1M}(\Phi, \vec{J}, \Phi^*, \vec{J}^*) &= (\sigma_a \Phi, \Phi^*)_{\mathcal{D}} + (3\sigma_{tr} \vec{J}, \vec{J}^*)_{\mathcal{D}} + (\vec{\nabla} \Phi, \vec{J}^*)_{\mathcal{D}} - (\vec{J}, \vec{\nabla} \Phi^*)_{\mathcal{D}} \\ &+ \frac{1}{4} ([[\Phi]], [[\Phi^*]])_{E_h^i} + ([[\Phi]], \{\{\vec{J}^* \cdot \vec{n}\}\})_{E_h^i} - (\{\{\vec{J} \cdot \vec{n}\}\}, [[\Phi^*]])_{E_h^i} \\ &+ ([[\vec{J} \cdot \vec{n}]], [[\vec{J}^* \cdot \vec{n}]])_{E_h^i} \\ &+ \frac{1}{4} (\Phi, \Phi^*) + \frac{1}{2} (\vec{J} \cdot \vec{n}, \Phi^*)_{\partial \mathcal{D}^v} - \frac{1}{2} (\Phi, \vec{J}^* \cdot \vec{n})_{\partial \mathcal{D}^v} \\ &+ 2(\vec{J} \cdot \vec{n}, \vec{J}^* \cdot \vec{n})_{\partial \mathcal{D}^r} \end{aligned} \quad (27)$$

$$l(\Phi^*, \vec{J}^*) = (Q_0, \Phi^*)_{\mathcal{D}} + (3\vec{Q}_1, \vec{J}^*)_{\mathcal{D}} \quad (28)$$

We can see a few differences related to edge integrals between the P1C and P1M. On interior edges, there is an additional term in the P1C form along the x - and y - directions. Also, the coefficients for these current terms are $\frac{9}{16}$ in the P1C form, whereas they are equal to 1 in the P1M form. Finally, current terms are present for the vacuum boundary in the P1C form but are absent in the P1M. The current coefficients for the reflecting boundary are $\frac{9}{4}$ in P1C while they are equal to 2 in P1M.

3. RESULTS

A 2-D rectangular domain is cut into 2 triangular cells. All four boundaries are reflecting boundaries. The size of the domain can vary with x and y . The total cross section for the 2 cells, denoted by $\bar{\sigma}_{t,1}$, $\bar{\sigma}_{t,2}$, the scattering ratio c_1 , c_2 and the average scattering cosine $\bar{\mu}_{0,1}$, $\bar{\mu}_{0,2}$ can be varied in the two cells (i.e., heterogeneous domain). Linear finite elements are used. An S_8 level-symmetric angular quadrature is employed. The spectral radii of the source iteration (SI) procedure and the SI with DSA procedures are calculated as the maximum eigenvalue of the source iteration matrix with or without DSA.

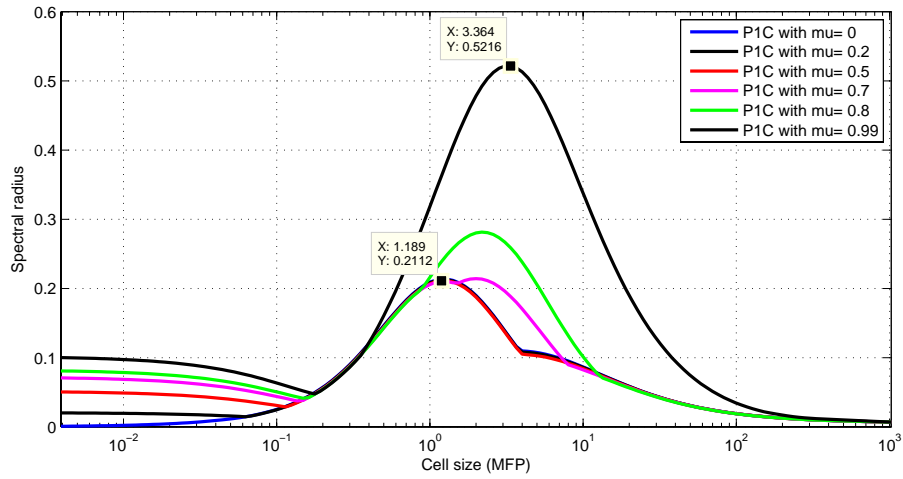


Figure 1. Spectral radius for the P1C form

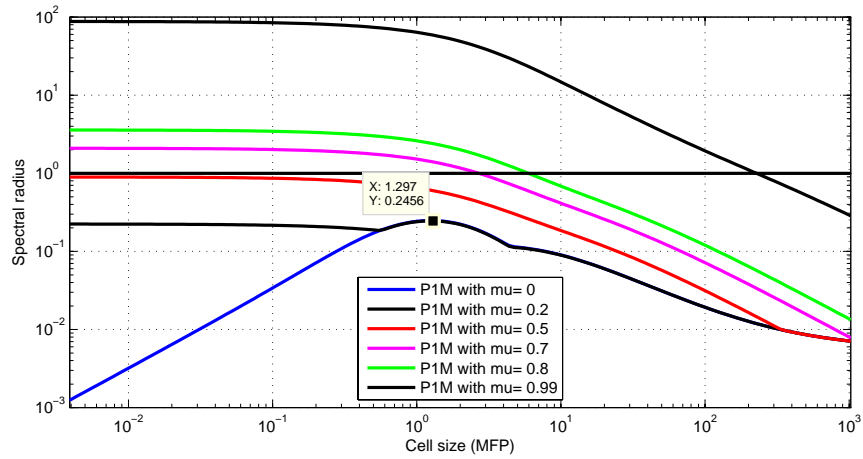


Figure 2. Spectral radius for the P1M form

We test the two DSA schemes, DSA-P1C and DSA-P1M, for various values of total cross sections (in this example, $\sigma_{t,1} = \sigma_{t,2}$, $c_1 = c_2 = 0.9999$) with a fixed domain size $x = y = 1cm$. Various average scattering cosines from 0 (isotropic) to 0.99 with $\bar{\mu}_{0,1} = \bar{\mu}_{0,2}$) are tested. Figs. 1 and 2 present these results.

4. CONCLUSIONS AND FUTURE WORK

In this paper, we presented two forms of DSA equations based on the P_1 approximation. One form, DSA-P1C, was strictly derived from the DGFEM form of the S_N transport equation by assuming a linear angular dependence of the angular flux; the other form, DSA-P1M, is based on Ref. [2] and employs specific numerical (flux) definitions for the scalar flux and net currents at the cell interfaces. A simple test problem was performed, with and without anisotropic scattering, to assess the performance of these two forms of DSA; even though the two forms are relatively similar, significant differences in the spectral radius can be observed. We currently are developing a the Fourier analysis of DSA-P1C and its implementation within a mesh adaptive transport solver.

REFERENCES

- [1] Marvin L. Adams, Edward W. Larsen, "Fast iterative methods for discrete-ordinates particle transport calculations", Progress in Nuclear Energy, Volume 40, Issue 1, 3-159 (2002).
- [2] James S. Warsa, Todd A. Wareing, Jim E. Morel, "Fully Consistent Diffusion Synthetic Acceleration of Linear Discontinuous SN Transport Discretizations on Unstructured Tetrahedral Meshes", Nucl. Sci. Engr., 141, 236–251 (2002).
- [3] Discontinuous Galerkin Methods: Theory, Computation and Applications, (Lecture Notes in Computational Science and Engineering, volume 11) by Bernardo Cockburn, G. Karniadakis and C. Shu (Editors), Springer-Verlag, New York (2000).
- [4] Benjamin Stamm, "Spectral Discontinuous Galerkin Method for Hyperbolic Problems", Master project, EPFL, Lausanne (2005).
- [5] Douglas N. Arnold, Franco Brezzi, Bernardo Cockburn, L. Donatella Marini, "Unified Analysis of Discontinuous Galerkin Methods for Elliptic Problems", SIAM J. Numer. Anal., 39, 5, 1749-1779 (2002).